Journal of Engineering Science and Technology
Vol. 5, No. 4 (2010) 426 - 434

ANALYSIS FOR AERODYNAMICS OF THE SIMPLIFIED MODEL OF A COMMERCIAL AIRPLANE CRUISING AT TRANSONIC SPEED

KIM YANGKYUN[1], KIM SUNGCHO[2,*]

[1]Division of Mechanical and Space Eng., Hokkaido University, 060-8628, Japan
[2]Mechanical and Aerospace Eng., Sunchon National University, 540-742, Korea
*Corresponding Author: ksc@sunchon.ac.kr

Abstract

This paper describes the computational analysis and visualization of flow around the model of a commercial airplane, Boeing 747-400. The geometry was realized through reverse engineering technique based on the photo scanning measurement. The steady three-dimensional viscous compressible governing equations were solved in the unstructured grid system. The basic conditions for computation were chosen as the same to those of Boeing 747-400's cruising state. The high Reynolds turbulence models are tried. The angle of attack is varied to investigate the effect of the flight conditions to the aerodynamic performance. And flow and aerodynamic characteristics due to the existence of winglet were compared.

Keywords: Aerodynamic coefficients, Wingtip vortex, Winglet, Visualization.

1. Introduction

Airplanes are analyzed with various design approach and computational method. In the process through the conceptual design of an aircraft, preliminary and detailed design aerodynamic analyses should be accomplished in the configuration of main wing, tail wing, fuselage, landing gear and selection of high lift device considering performance, stability and attitude control. Cost and time are highly spent in the initial stage of design process because of frequent design modification.

Thus, in the primary development for obtaining the quick results, the effects of a wing variation such as aspect ratio, taper ratio, sweepback angle, etc. are examined by experience based on the generalized experiment, flight data and theory. Especially, aerodynamic characteristics of an airplane shape in the initial design process is analyzed on whether or not agreement with theory and stability

Nomenclatures

AOA	Angle of attack, deg.
C_D	Drag coefficient
C_L	Lift coefficient
C_P	Pressure coefficient
H	Enthalpy, m^2/s^2
K	Turbulence kinetic energy, m^2/s^2
p	Pressure of fluid, Pa
q_j	Heat flux, W/m^2
R	Gas constant, m^2/s^2K
SA	Sparlart & Allmaras turbulence model
SST	Shear stress transport turbulence model
T	Absolute temperature, K
u_i	Velocity component, m/s
x_i	Cartesian coordinate

Greek Symbols

ε	Turbulent dissipation rate, m^2/s^3
μ	Viscosity, kg/ms
ρ	Density of fluid, kg/m^3
τ_{ij}	Component of stress tensor, kg/ms^2

through the wind tunnel tests and the geometries are often changed optimally during the repeated design cycle.

The wind tunnel tests are difficult and limited to experiment the real airplane under the actual flight condition. Thus computational aerodynamic analysis for supplementation of the physical tests has been a useful tool.

Boppe [1] et al. studied flow about the configuration combined fuselage with wing, and Ashley [2] et al. evaluated aerodynamic performance of wings and bodies. Despite the fact that there have been tons of researches on aerodynamics of the aircraft elements, however, the work on the full configuration is rare.

Accordingly, the topic in this paper is focused to investigate the flow field and the aerodynamic characteristics for the model of a commercial passenger airplane, Boeing 747-400. The full geometry is realized with the reverse engineering based on the photographic measurements [3]. Numerical computation is executed when she flies at the transonic cruising speed with varying the angle of attack and turbulence model. And the effect of winglet on the flow field is described.

2. Numerical Computation

The steady three-dimensional viscous compressible flow is solved numerically. The governing equations consist of the continuity, momentum, energy equations and the equation of state, and are briefly described as follows

$$\frac{\partial \rho u_j}{\partial x_j} = 0 \tag{1}$$

$$\frac{\partial \rho u_i u_j}{\partial x_j} = \frac{\partial p}{\partial x_i} + \frac{\partial \tau_{ij}}{\partial x_j} \tag{2}$$

$$\frac{\partial \rho u_j h}{\partial x_j} = -\frac{\partial p u_j}{\partial x_j} + \frac{\partial (u_i \tau_{ij} - q_j)}{\partial x_j} \tag{3}$$

$$p = \rho RT \tag{4}$$

where ρ is the density of fluid, p is the pressure of fluid, u_i is the velocity component, x_i is the Cartesian coordinate, h is the enthalpy, τ_{ij} is the component of stress tensor, R is the gas constant, T is the absolute temperature.

The computational work was done using STAR-CD and the grid system was generated in ICEMCFD. The flow field was computed by the finite volume method which could follow well the boundary conditions in the unstructured grid. The convective terms in the governing equations were treated by the Crank-Nicholson method and the spatial discretization method adopting the 1st order upwind scheme.

The basic flight conditions for computation were same to those of Boeing 747-400's cruising, i.e., the atmospheric condition at 13 km above the sea level and Mach number of 0.85. The freestream approaches to the aircraft, the airplane surface is no-slip, and the pressure conditions are applied on the all remaining boundaries. The high Reynolds number k-ε model and standard wall function are applied for the turbulence, and other several turbulence models were considered for comparison. The computational domain, selected by half due to the symmetry of the airplane, consists of the unstructured hexahedron grids. The grids on the region where the flow seems to be changed severely are sufficiently dense.

3. Results and Discussion

The convergence was decided when all the physical quantities varied below 10^{-6} as well the aerodynamic forces did not change.

Figure 1 shows the pressure distribution, streamlines based on Mach number, wing-tip vortices and density distribution just behind main wings when the angle of attack is 0° and Mach number is 0.85. Relatively high pressures distribute near the stagnation regions, i.e., at the fuselage nose, the front junction of the wings and the fuselage, the leading edge of the wing, and the front part of the engine cowling. The stagnation pressure generated at the fuselage front decreases as the flow accelerates downstream moving along the surface. And relatively high pressure generates in front of the cockpit and relatively low pressure is distributed widely behind the cockpit due to the flow acceleration.

The pressure on the upper surface of the swept wing is lower near the wing tip than the other parts. The secondary velocity components which are normal to the main stream-wise direction show that the strong wingtip vortex due to the roll-up behind the winglet was generated. Although Boeing 747-400 has adopted winglets to reduce the induced drag, considerable wingtip vortices were generated.

These phenomena will be referred later. Also this figure shows that the acceleration region on the upper wing surface and considerable distortion in the flow near the engines through the streamlines. In particular, the streams passing the engine mount and flowing over the upper wing surface severely move toward the wing-root.

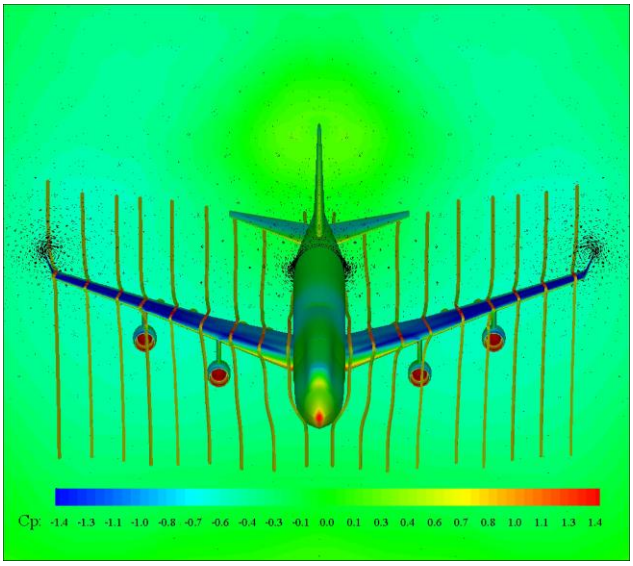

Fig. 1. Surface Pressure, Stream Line, and Wingtip Vortex at the Cruising Condition.

To predict aerodynamic characteristics and stall point which heavily affects the flight performance and stability, computation was conducted from -20° to 27° of the angle of attack in cruising Mach number 0.85 equivalent to transonic flow (Fig. 2). And the differences in aerodynamics are discussed as the turbulence model is different. Main turbulence model used in computation is the high Reynolds number k-ε model with applied general coefficients, additionally RNG k-ε, high Reynolds number Sparlart & Allmaras, high Reynolds number k-ω, Chen's k-ε and k-ω SST (shear stress transport) models were also tried for comparison.

Figure 2 shows that lift coefficient rapidly decreases at 18° of the angle of attack after it increased linearly up to 17° when the high Reynolds number k-ε model was employed. And when the SST k-ω and Sparlart & Allmaras models were applied, lift coefficient started to be reduced between 16° and 17°, 18° and 19° respectively. It means that stall directly related to the airplane stability is generated by flow separation on the upper wing surface.

Marvin [4] made experiments on the improvement of the aerodynamic performance in high angle of attack and stall angle through the wind tunnel test for preventing dangerous stall of an airplane by using flaps and aileron. When the high Reynolds number k-ε model was employed, the minimum drag was observed around -2° of the angle of attack, and an abrupt drag rise i.e., stall was predicted at just after 18°. Bardina [5] concluded that the SST model in turbulence has the best performance in transonic flow computation compared with the second-order equations like k-ε and k-ω models, and the Spalart & Allmaras model is better. In this result as seen in Fig. 2, however, the SST model predicts lower aerodynamic

value than other models in high angle of attack, and the largest aerodynamic forces were resulted by the Chen's model.

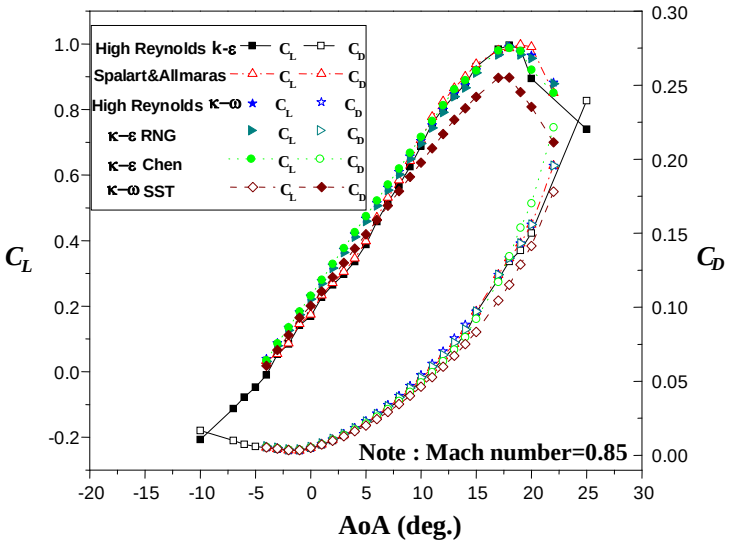

Fig. 1. Aerodynamic Coefficients at Mach Number 0.85 versus Angle of Attack and Turbulence Model.

To find out in detail the aerodynamic phenomena on the wing surface, pressure distribution along the wing chord at the 0, 20, 40, 75, and 95% wing sections from the wing root toward the wing tip are plotted in Figs. 3-6 as a function of angle of attack like researches of David et al. [6], Lee-Rausch and Frink [7], and Rumsey et al. [8]. The reference angles of attack are -5°, 0°, 5°, 14°, and 20°, and the Mach number is 0.85 just as the cruising condition.

As seen in Fig. 3 pressure distributions on the upper and lower wing surfaces are reversed each other at -5° of the angle of attack which is below or less than the zero lift angle (approximately -2°). Since the area between the pressure curves for the upper and lower wing surfaces had meaning like lift force, lift is nearly not produced over all regions at -5°.

Despite no near sonic rooftop at the 0% span of the 0° (Fig. 4), the aerodynamic loading at the leading edge is small and the pressure is restored rapidly near the trailing edge. That is similar to Martin's results [9] of calculating the ONERA M6 wing. In his study, because flow separation generated by interference between fuselage and wing affects the flow near the wing root, low pressure region between the leading and trailing edges at the root section on the upper wing surface does not appear.

The pressure distribution at 20% of the span length from root to tip presents that the flow acceleration occurred in x/c = 0.0-0.18(x: measured from the leading edge, c: the wing chord length) and pressure is recovered in x/c = 0.88~1.0. This means that week shock wave structure is observed in x/c = 0.88~1.0 along the

wing chord. The pressure distribution at 40% and 75% of the span length from root to tip indicates that flow acceleration occurred rapidly and pressure recovery region is widely distributed as compared with 20% of the span length from root to tip because of the effect of wing sweepback angle and propulsion system.

Pressure area at 95% of the span length from root to tip is large although this spanwise location is near the wing tip. The reason seems to be related to the fact that winglet affects to reduce drag at place of wing tip [9].

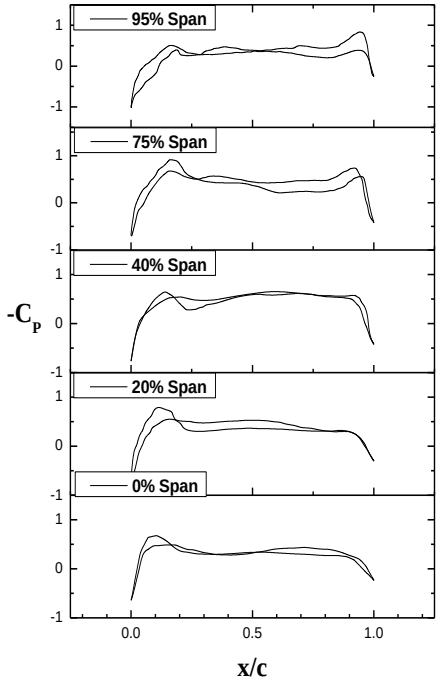

Fig. 3. Pressure Distribution from the Wing Root toward the Wing Tip at -5°.

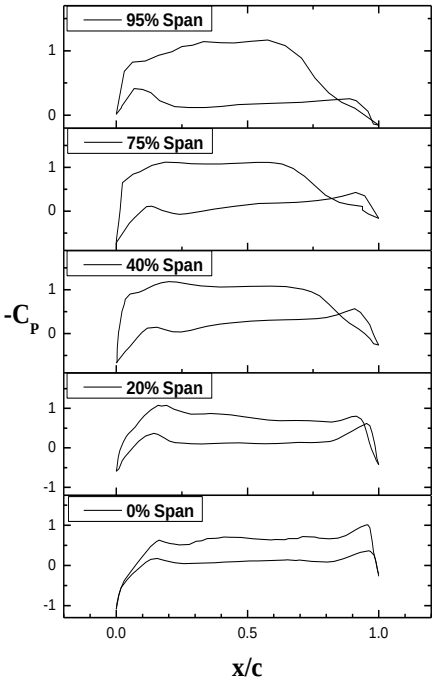

Fig. 4. Pressure Distribution from the Wing Root toward the Wing Tip at 0°.

Figures 5 and 6 are for 5° and 15° of the angle of attack. Here, lift area as pressure difference between upper and lower surface is extended in comparison with low angle. And flow acceleration rapidly occurred near the leading edge.

For understanding wing tip flow pattern closely, Fig. 7 shows velocity magnitude, i.e. secondary flow pattern, on the plane normal to the flight direction, at the location from the trailing edge by 0, 1 and 5 times of the chord length of the wing end (or tip) in condition of cruising Mach number 0.85 and 0° of the angle of attack. In Fig. 7(a), just behind the wing, airplane with winglet generates smaller vortex than that with no-winglet. Induced drag is results that fluid loses the energy by the generation of wing-tip vortex, namely that wing with winglet gets the effect of reducing the induced drag because the smaller the tip vortex, the smaller the induced drag. Figures 7(b)-(d) present the secondary flow patterns behind 1, 2 and 5 times of the wing tip cord length from the trailing edge. The vortex strength of both cases weakens according to going downstream, but they exist in far field. So it is necessary to study the optimal configuration of winglet for minimum induced drag.

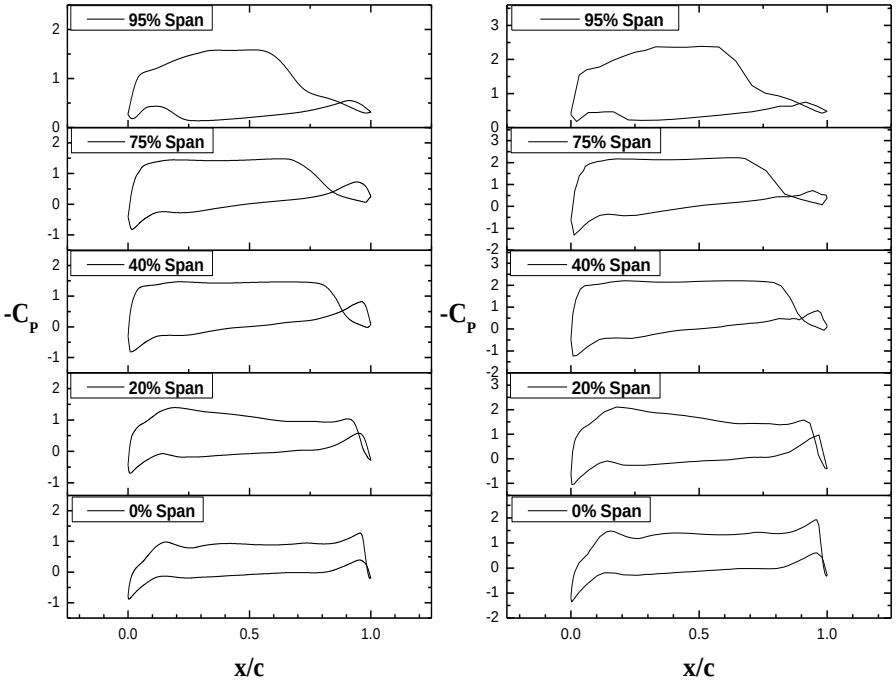

Fig. 5. Pressure Distribution from the Wing Root toward the Wing Tip at 5°.

Fig. 6.Pressure Distribution from the Wing Root toward the Wing Tip at 15°.

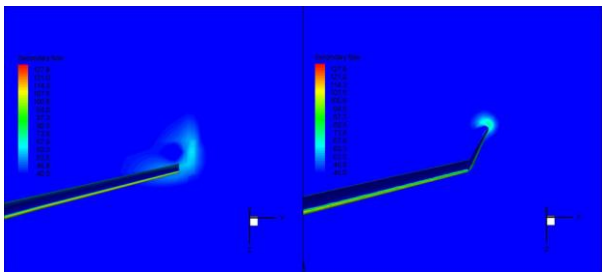

(a) 3 times

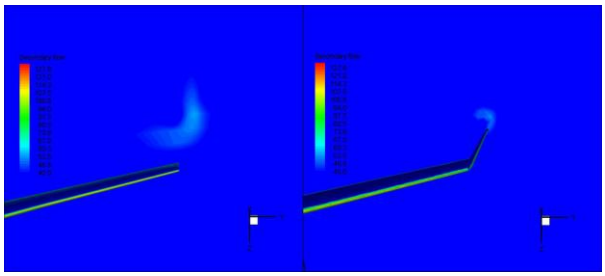

(b) 5 times

Fig. 2. Wing Tip Vortices with or without Winglet at the Location from the Trailing Edge by Several Times of the Wing-Tip Chord Length.

Figure 8 shows the effect of winglet on aerodynamic characteristics in 0°-10° of the angle of attack. Figure 8(a) shows that lift coefficients with winglet are increased by 6.89% and 11.9%, respectively when the angle of attack is 0° and 10°. This means that the winglet is more effective at the high angles of attack, or the gradient of the lift coefficient becomes large due to winglet. Drag coefficients of the airplane with winglet is about 0.8% larger than that without winglet when the angle of attack is 0° (not clearly seen in Fig. 8(b)). The differences in drag coefficients are little up to 5°, but after that differences appear to reach 6.1% at 10°. As mentioned above, this result indicates that induced drag was decreased by adopting winglet.

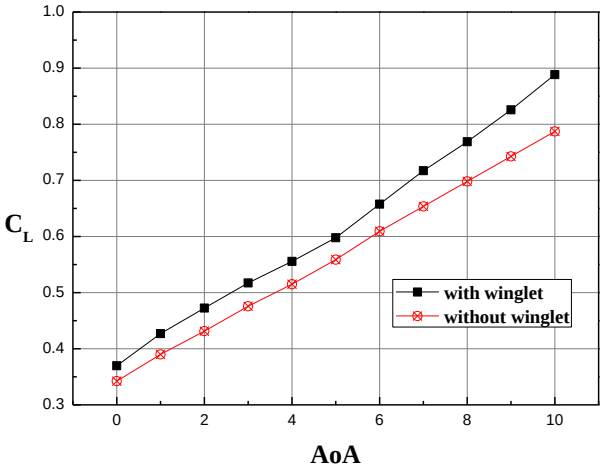

(a) Lift Coefficient.

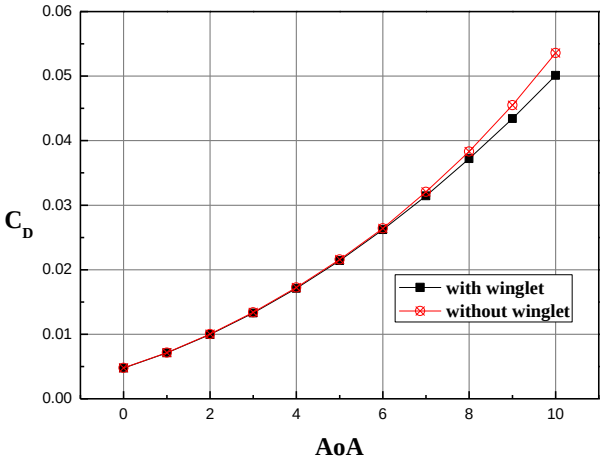

(b) Drag Coefficient.

Fig. 8. Effect of the Winglet on Aerodynamic Coefficients as a Function of the Angle of Attack.

4. Conclusion

In this study, the airplane configuration of Boeing 747-400 was realized by reverse engineering based on the non-contact photographic measurements for its model and conclusion was obtained by numerical computation of viscous flows around the airplane in transonic speed.

The pressure distribution is estimated on the aircraft surfaces, and the pressure is high where the stagnation flows exist, i.e., at the nose of the fuselage, and discontinuous region near the cockpit. The pressure coefficients at the several spanwise locations on the wing surface are observed; pressure load near the leading edge at the wing root is small, weak shock wave phenomena are shown near the wing root, and rapid acceleration and pressure recovery are generated near the leading and trailing edges, respectively.

Maximum lift coefficient appears at 18° of the angle of attack and minimum drag coefficient at the -2°.

And k-ω SST model predicts relatively low aerodynamic values and Chen's model predicts the highest values at high angle of attack.

References

1. Boppe, C.W. (1980). Transonic flow field analysis for wing-fuselage configurations. *NASA-CR-3243*.
2. Ashley, H.; and Landahl, M. (1965). *Aerodynamics of wings and bodies*. Reading MA, Massachusetts, Addison-Wesley Publishing Company Co., Inc.
3. Kim, Y.K.; Kim, S.; Choi, J.; and Kim, J.S. (2006). Geometry realization of an aircraft by reverse engineering based on photo images. *Sunchon National Univ. J.*, 25, 189-194.
4. Fink, M.P.; Shivers, J.P.; White, L.C. (1974). Wind-tunnel tests of a full-scale model of a light twin-engine airplane with fixed auxiliary airfoil or leading-edge slot. *NASA TN D-7474*.
5. Bardina, J.E.; Huang, P.G; and Coakley, T.J. (1997). Turbulence modeling validation. *AIAA-97-2121*.
6. David, L.T. et al. (2002). Summary of data from the firs AIAA CFD drag prediction workshop. *AIAA-2002-0841*.
7. Lee-Rausch, E.M.; Frink, N.T.; Mavriplisb, D.J.; Rauscha, R.D.; and Milholena, W.E. (2009). Transonic drag prediction on a DLR-F6 transport configuration using unstructured grid solvers. *Computers & Fluids*, 38(3), 511-532.
8. Rumsey, C.L.; Rivers, S.M.; and Morrison, J.H. (2005). Study of CFD variation on transport configurations from the second drag-prediction workshop. *Computers & Fluids*, 34(7), 785-816.
9. Martin, G. (2006). *Comparison of aerodynamic performance of raked wing tips and large winglets*. Master thesis, Cranfield University.